# 857. Experimental study for structural damage identification with incomplete measurements

**Rui Li[1], Li Zhou[2], Jann N. Yang[3]**
[1, 2]State Key Laboratory of Mechanics and Control of Mechanical Structures
Nanjing University of Aeronautics and Astronautics, No. 29 Yudao Street, Nanjing 210016, China
[3]Department of Civil & Environmental Engineering, University of California, Irvine, CA 92697, USA
[2]Corresponding author
**E-mail:** [1]*lirui@nuaa.edu.cn*, [2]*lzhou @nuaa.edu.cn*, [3]*jnyang@uci.edu*
*(Received 30 May 2012; accepted 4 September 2012)*

**Abstract.** Finite element formulation for the equation of motion should be used for identification of local damage of a structure at the element level. However, the finite element model of a structure involves a large number of degrees of freedom and requires a large number of sensor measurements. To avoid measuring vibration responses, which are difficult to obtain (e.g. rotational accelerations), and to reduce the required number of sensors, a reduced-order finite element formulation along with the adaptive sequential nonlinear least square estimation technique is proposed in this paper to identify local damages of structures. To verify the applicability and effectiveness of the proposed approach, two series of damage detection experiments were conducted using scaled cantilever beams. One series of experimental tests were conducted for the detection of constant damages. In this test series, different damage severities were simulated by drilling different number of circular holes with different sizes in a particular element of a cantilever beam. Another series of experimental tests were conducted to verify the online damage tracking capability of the proposed approach. In this test series, a stiffness element device was installed in a particular element of another cantilever beam to simulate the abrupt stiffness reduction of that element during the test. Experimental results demonstrate that the proposed reduced-order finite element model along with the adaptive sequential nonlinear least square estimation technique is effective and accurate in detection of structural damages, including the damage location and severity using only a limited number of sensors.

**Keywords:** experimental study, damage detection, structural health monitoring, system identification, adaptive sequential nonlinear least square estimation.

## 1. Introduction

The purpose of structural health monitoring systems is to identify the state of the structure and to detect the damage when it occurs. In this regard, analysis methodologies for structural damage identification, based on measured vibration data, have been thoroughly studied [1-3]. However, most of the available methods require both the reference data (the data of the structure without damage) and the data after damage. Further, these methods are capable of identifying only the constant system parameters, such as stiffness, and the damage is obtained by a comparison of the constant structural parameters prior to and after the damage. In practice, however, after a severe event, such as a strong earthquake, it may not be feasible to conduct vibration tests to obtain meaningful data for damage identifications. To detect structural damage based on the vibration data measured during a severe event, such as a strong earthquake, time-domain approaches have been studied and developed, such as the least-square estimation (LSE) [4-8], the extended Kalman filter (EKF) [9-12], the Monte Carlo filter [13, 14], the sequential prediction error method [15, 16], and others [17].

Recently, a new time-domain damage tracking approach, referred to as the adaptive sequential nonlinear least square estimation (ASNLSE), has been proposed [18, 19], and it has been demonstrated to be quite effective in identifying structural damages based on simulation results. However, no experimental study was conducted for the verification of this technique.

Further, to detect local structural damages quantitatively, such as the degradation of stiffness of an element, a finite element (FE) formulation is required. However, FE model of a structure involves a large number of degrees of freedom (DOFs) and requires a large number of sensor measurements. From the practical point of view, it is highly desirable to install as few vibration sensors as possible. Likewise, some vibration quantities are difficult to measure, such as the rotational acceleration at a nodal point. To avoid the need for measuring vibration responses which are difficult to measure, and to reduce the required number of sensors, the static condensation method is used in this paper to reduce the dimension of the FE-based equations of motion.

In this paper, the adaptive sequential nonlinear least square estimation (ASNLSE) technique [18-19] along with the reduced-order FE formulation is proposed to identify the local damages of structures, and experimental tests are conducted to verify the capability of the proposed damage detection approach. First, a series of experimental tests were performed using a scaled cantilever beam. The beam was subject to the external white noise excitations. In this test series, different severities of damages for the beam were simulated by drilling different number of circular holes with different sizes in a particular element of the cantilever beam. Further, a second series of experimental tests were conducted using another cantilever beam to verify the online damage tracking capability of the proposed approach. In this test series, a stiffness element device (SED) was installed on the beam to simulate the abrupt reduction of the stiffness of the damaged element during the experimental tests. Based on the proposed approach and limited number of measured vertical acceleration data (without rotational response measurements), the stiffness of all finite elements of the beam were identified. The capability and accuracy of the proposed reduced-order FE formulation along with the adaptive sequential nonlinear least square estimation (ASNLSE) technique [18-19] in identifying structural damages will be demonstrated experimentally.

## 2. Adaptive sequential nonlinear least square estimation

### 2. 1 Equation of motion based on reduced-order FE model

Based on the FE formulation, the vector equation of motion of a $s$-DOF linear structure can be expressed as:

$$\underline{\mathbf{M}}\ddot{\mathbf{x}}(t)+\underline{\mathbf{C}}\dot{\mathbf{x}}(t)+\underline{\mathbf{K}}\mathbf{x}(t)=\underline{\boldsymbol{\eta}}\mathbf{f}(t) \tag{1}$$

in which $\mathbf{x}(t)=[\underline{x}_1(t),\ \underline{x}_2(t),\ \ldots,\ \underline{x}_s(t)]^{\mathrm{T}}=s$ - displacement vector; $\underline{\mathbf{M}}=(s\times s)$ mass matrix; $\underline{\mathbf{C}}=(s\times s)$ damping matrix; $\underline{\mathbf{K}}=(s\times s)$ stiffness matrix; $\underline{\boldsymbol{\eta}}=(s\times(\bar{m}+r))$ excitation influence matrix and $\underline{\mathbf{f}}(t)=(\bar{m}+r)$ - excitation vector. The dimension $s$ of the FE formulation in Eq. (1) is very large so that: (i) the computational efforts for the determination of all unknown parameters, such as $\underline{\mathbf{C}}$ and $\underline{\mathbf{K}}$, are quite involved, and (ii) the required number of sensors is large. To overcome these challenges, the number of equations of motion in Eq. (1) can be reduced by using the static condensation method as follows. First, divide the displacement vector $\mathbf{x}(t)=[\underline{x}_1(t),\ \underline{x}_2(t),\ \ldots,\ \underline{x}_s(t)]^{\mathrm{T}}$ into two vectors, i.e., $\mathbf{x}(t)$ and $\mathbf{x}^*(t)$, where $\mathbf{x}(t)=[x_1(t),\ x_2(t),\ \ldots,\ x_m(t)]^{\mathrm{T}}$ is an $m$-dimensional displacement vector representing the primary degrees of freedom system, and $\mathbf{x}^*(t)=[x_1^*(t),\ x_2^*(t),\ \ldots,\ x_{s-m}^*(t)]^{\mathrm{T}}$ denotes the secondary degrees of freedom to be condensed. Based on the method of static condensation [20, 21], Eq. (1) can be condensed into an $m$-DOF system as follows:

$$\mathbf{M}(\boldsymbol{\theta})\ddot{\mathbf{x}}(t)+\mathbf{C}(\boldsymbol{\theta})\dot{\mathbf{x}}(t)+\mathbf{K}(\boldsymbol{\theta})\mathbf{x}(t)=\boldsymbol{\eta}_1\underline{\mathbf{f}}(t) \tag{2}$$

in which $\mathbf{M}(\boldsymbol{\theta})$, $\mathbf{C}(\boldsymbol{\theta})$ and $\mathbf{K}(\boldsymbol{\theta})$ are $(m\times m)$ condensed mass, damping and stiffness matrices, respectively, and $\boldsymbol{\eta}_1$ is a $(m\times(\bar{m}+r))$ excitation influence matrix. In Eq. (2), $\boldsymbol{\theta}=[\theta_1,\ \theta_2,\ \ldots,\ \theta_n]^{\mathrm{T}}$ is an $n$ - unknown parametric vector with $\theta_i$ $(i=1,\ 2,\ \ldots,\ n)$ being the $i^{\text{th}}$ unknown parameter of the entire structure, including damping, stiffness and other parameters of the original finite-element system in Eq. (1). Further, the $(\bar{m}+r)$ - excitation vector $\underline{\mathbf{f}}(t)$ is divided into two vectors, denoted by $\mathbf{f}^*(t)$ and $\mathbf{f}(t)$, respectively, where $\mathbf{f}^*(t)=r$ - unknown (or unmeasured) excitation vector and $\mathbf{f}(t)=\bar{m}$ - known (or measured) excitation vector. Then, Eq. (2) can be expressed as:

$$\mathbf{M}(\boldsymbol{\theta})\ddot{\mathbf{x}}(t)+\mathbf{C}(\boldsymbol{\theta})\dot{\mathbf{x}}(t)+\mathbf{K}(\boldsymbol{\theta})\mathbf{x}(t)=\boldsymbol{\eta}^*\mathbf{f}^*(t)+\boldsymbol{\eta}\mathbf{f}(t) \tag{3}$$

in which $\boldsymbol{\eta}^*$ is a $(m\times r)$ excitation influence matrix for $\mathbf{f}^*(t)$, and $\boldsymbol{\eta}$ is a $(m\times\bar{m})$ excitation influence matrix for $\mathbf{f}(t)$. Note that Eq. (3) is a general equation in which $\bar{m}=0$ if no excitation is measured and $r=0$ if all excitations are measured. In what follows, the bold face letter represents either a vector or a matrix.

Since Eq. (3) is no longer a linear function of the unknown parametric vector $\boldsymbol{\theta}$, it is first discretized at $t=t_{k+1}=(k+1)\Delta t$ with $\Delta t$ being the sampling time. Then, the discretized equation is linearized with respect to $\boldsymbol{\theta}$ around $t=t_k=k\Delta t$ with the results:

$$\boldsymbol{\varphi}(\mathbf{X}_{k+1})\boldsymbol{\theta}_{k+1}=\boldsymbol{\eta}^*\mathbf{f}^*_{k+1}+\mathbf{y}_{k+1} \tag{4}$$

where:

$$\boldsymbol{\varphi}(\mathbf{X}_{k+1})=\left[\partial\mathbf{L}/\partial\boldsymbol{\theta}\right]_{\boldsymbol{\theta}=\boldsymbol{\theta}_k},\ \mathbf{y}_{k+1}=\boldsymbol{\eta}\mathbf{f}_{k+1}-\mathbf{L}(\boldsymbol{\theta}_k)+\left[\partial\mathbf{L}/\partial\boldsymbol{\theta}\right]_{\boldsymbol{\theta}=\boldsymbol{\theta}_k}\boldsymbol{\theta}_k \tag{5}$$

$$\mathbf{L}=\mathbf{M}(\boldsymbol{\theta}_k)\ddot{\mathbf{x}}_{k+1}+\mathbf{C}(\boldsymbol{\theta}_k)\dot{\mathbf{x}}_{k+1}+\mathbf{K}(\boldsymbol{\theta}_k)\mathbf{x}_{k+1} \tag{6}$$

in which $\boldsymbol{\varphi}(\mathbf{X}_{k+1})=\boldsymbol{\varphi}[\mathbf{X}(t_{k+1});t_{k+1}]$, $\boldsymbol{\theta}_{k+1}=\boldsymbol{\theta}(t_{k+1})$, $\mathbf{y}_{k+1}=\mathbf{y}(t_{k+1})$, and $\mathbf{X}_{k+1}=[\mathbf{x}^{\mathrm{T}}_{k+1},\dot{\mathbf{x}}^{\mathrm{T}}_{k+1}]^{\mathrm{T}}$ is the state vector.

### 2. 2 Adaptive sequential non-linear least-square estimation

A recently proposed structural damage detection technique [18, 19], referred to as the adaptive sequential non-linear least-square estimation (ASNLSE), will be used for the detection of damages. Instead of estimating unknown vectors $\mathbf{X}_k$ and $\boldsymbol{\theta}_k$ simultaneously, the ASNLSE approach [18, 19] estimates $\mathbf{X}_k$ and $\boldsymbol{\theta}_k$ in two steps. The first step is to determine $\boldsymbol{\theta}_k$ by assuming that $\mathbf{X}_k$ is given using the LSE solution. The second step is to determine $\mathbf{X}_k$ through a non-linear LSE approach, referred to as the ASNLSE, as follows.

Step I: With the assumption that the state vector $\mathbf{X}_k$ is known and the parametric vector $\boldsymbol{\theta}_k$ is constant, the recursive solution for $\hat{\boldsymbol{\theta}}_{k+1}$ that is the estimate of $\boldsymbol{\theta}_{k+1}$ is given by:

$$\hat{\boldsymbol{\theta}}_{k+1}=\hat{\boldsymbol{\theta}}_k+\mathbf{K}_{\boldsymbol{\theta},k+1}(\mathbf{X}_{k+1})[\mathbf{y}_{k+1}-\boldsymbol{\varphi}_{k+1}(\mathbf{X}_{k+1})\hat{\boldsymbol{\theta}}_k+\boldsymbol{\eta}^*\hat{\mathbf{f}}^*_{k+1|k+1}] \tag{7}$$

$$\hat{\mathbf{f}}^*_{k+1|k+1}=-\mathbf{S}_{k+1}(\mathbf{X}_{k+1})(\boldsymbol{\eta}^*)^{\mathrm{T}}[\mathbf{I}-\boldsymbol{\varphi}_{k+1}(\mathbf{X}_{k+1})\mathbf{K}_{\boldsymbol{\theta},k+1}(\mathbf{X}_{k+1})]\times[\mathbf{y}_{k+1}-\boldsymbol{\varphi}_{k+1}(\mathbf{X}_{k+1})\hat{\boldsymbol{\theta}}_k] \tag{8}$$

$$\mathbf{K}_{\boldsymbol{\theta},k+1}(\mathbf{X}_{k+1})=(\boldsymbol{\Lambda}_{k+1}\mathbf{P}_{\boldsymbol{\theta},k}\boldsymbol{\Lambda}^{\mathrm{T}}_{k+1})\boldsymbol{\varphi}^{\mathrm{T}}_{k+1}(\mathbf{X}_{k+1})[\mathbf{I}+\boldsymbol{\varphi}_{k+1}(\mathbf{X}_{k+1})(\boldsymbol{\Lambda}_{k+1}\mathbf{P}_{\boldsymbol{\theta},k}\boldsymbol{\Lambda}^{\mathrm{T}}_{k+1})\boldsymbol{\varphi}^{\mathrm{T}}_{k+1}(\mathbf{X}_{k+1})]^{-1} \tag{9}$$

$$\mathbf{S}_{k+1}(\mathbf{X}_{k+1})=\{(\boldsymbol{\eta}^*)^{\mathrm{T}}[\mathbf{I}-\boldsymbol{\varphi}_{k+1}(\mathbf{X}_{k+1})\mathbf{K}_{\boldsymbol{\theta},k+1}(\mathbf{X}_{k+1})]\boldsymbol{\eta}^*\}^{-1} \tag{10}$$

$$\mathbf{P}_{\boldsymbol{\theta},k}=[\mathbf{I}+\mathbf{K}_{\boldsymbol{\theta},k}(\mathbf{X}_k)\boldsymbol{\eta}^*\mathbf{S}_k(\mathbf{X}_k)(\boldsymbol{\eta}^*)^{\mathrm{T}}\boldsymbol{\varphi}_k(\mathbf{X}_k)][\mathbf{I}-\mathbf{K}_{\boldsymbol{\theta},k}(\mathbf{X}_k)\boldsymbol{\varphi}_k(\mathbf{X}_k)](\boldsymbol{\Lambda}_k\mathbf{P}_{k-1}\boldsymbol{\Lambda}^{\mathbf{T}}_k) \tag{11}$$

in which $\mathbf{K}_{k+1}(\mathbf{X}_{k+1})$ is the LSE gain matrix.

Step II: The recursive solution for $\hat{\mathbf{X}}_{k+1|k+1}$ that is the estimation of $\mathbf{X}_{k+1}$ can be obtained as:

$$\hat{\mathbf{X}}_{k+1|k+1} = \hat{\mathbf{X}}_{k+1|k} + \overline{\mathbf{K}}_{k+1}[\mathbf{y}_{k+1} - \hat{\mathbf{y}}_{k+1}(\hat{\mathbf{X}}_{k+1|k})] \tag{12}$$

$$\hat{\mathbf{X}}_{k+1|k} = \mathbf{\Phi}_{k+1,k}\hat{\mathbf{X}}_{k|k} + \mathbf{B_1}\ddot{\mathbf{x}}_k + \mathbf{B}_2\ddot{\mathbf{x}}_{k+1} \tag{13}$$

$$\overline{\mathbf{K}}_{k+1} = \overline{\mathbf{P}}_{k+1|k}\mathbf{\Psi}^{\mathrm{T}}_{k+1,k}[\mathbf{I} + \mathbf{\Psi}_{k+1,k+1}\overline{\mathbf{P}}_{k+1|k}\mathbf{\Psi}^{\mathrm{T}}_{k+1,k+1}]^{-1} \tag{14}$$

$$\overline{\mathbf{P}}_{k+1|k} = \mathbf{\Phi}_{k+1,k}\overline{\mathbf{P}}_{k|k}\mathbf{\Phi}^{\mathrm{T}}_{k+1,k} \tag{15}$$

$$\overline{\mathbf{P}}_{k|k} = \overline{\mathbf{P}}_{k|k-1} - \overline{\mathbf{K}}_k\mathbf{\Psi}_{k,k}\overline{\mathbf{P}}_{k|k-1} \tag{16}$$

In which:

$$\hat{\mathbf{y}}_i[\mathbf{X}_i(\hat{\mathbf{X}}_{k+1|k})] = \boldsymbol{\varphi}_i(\mathbf{X}_i)\hat{\boldsymbol{\theta}}_i(\mathbf{X}_i) = \boldsymbol{\varphi}_i[\mathbf{X}_i(\mathbf{X}_{k+1})]\hat{\boldsymbol{\theta}}_i[\mathbf{X}_i(\mathbf{X}_{k+1})] \tag{17}$$

$$\mathbf{\Phi}_{k+1,k} = \begin{bmatrix} \mathbf{I} & (\Delta t)\mathbf{I} \\ \mathbf{0} & \mathbf{I} \end{bmatrix}, \ \mathbf{\Psi}_{k+1,k+1} = \left.\frac{\partial \hat{\mathbf{y}}_{k+1}(\mathbf{X}_{k+1})}{\partial \mathbf{X}_{k+1}}\right|_{\mathbf{X}_{k+1}=\mathbf{X}_{k+1}(\hat{\mathbf{X}}_{k+1|k})} \tag{18}$$

$$\mathbf{B}_1 = \begin{bmatrix} (0.5-\beta)(\Delta t)^2\mathbf{I} \\ (1-\gamma)(\Delta t)\mathbf{I} \end{bmatrix}, \ \mathbf{B}_2 = \begin{bmatrix} \beta(\Delta t)^2\mathbf{I} \\ \gamma(\Delta t)\mathbf{I} \end{bmatrix} \tag{19}$$

where $\beta$ and $\gamma$ are parameters used in the Newmark-$\beta$ method (usually $\beta = 0.25$, $\gamma = 0.5$ are used).

## 3. Experimental studies for identification of constant damages

To demonstrate the applicability of the proposed approach for damage detection of structures, a series of experimental tests were conducted using a cantilever beam as shown in Figs. 1-2. In these series of tests, different numbers of circular holes with different sizes were drilled in the fourth finite element of the cantilever beam to simulate different damage severities. The cantilever beam was excited vertically at Node 1 (Figs. 1-2) and the vertical acceleration responses at all nodes were measured. Some of the measured acceleration response data and the proposed ASNLSE approach will be used to estimate the stiffness of each finite-element to identify the damage location and severity.

### 3. 1 Experimental setup

A steel cantilever beam as shown in Fig. 1(a) is used for this experiment. The undamaged beam is 1.5 m long and it has a cross-sectional area of 0.057×0.005 m$^2$. The first two natural frequencies of the test specimen are 1.8 Hz, and 11.5 Hz, respectively. The beam was divided into 6 evenly spaced nodal points, as shown in Fig. 2. Six acceleration sensors (PCB 3701G3FA3G) were installed at the six nodes to measure the vertical acceleration responses of all nodes. An actuator was used to apply a vertical excitation force at Node 1, and a force sensor (PCB 208C03) was used to measure the applied force.

Firstly, two small circular holes were drilled in the 4$^{th}$ finite-element of the beam to simulate a small damage (about 5 % reduction of the stiffness in the 4$^{th}$ element), referred to as Damage Scenario I, and experimental tests were conducted to obtain the acceleration response data for the damage prediction. Secondly, two small circular holes for Damage Scenario I were enlarged to simulate a more severe damage (about 10 % reduction of the stiffness in the 4$^{th}$ element), referred to as Damage Scenario II, and experimental tests were conducted. In a similar manner, lager damages were simulated by either increasing the number of circular holes or enlarging the size of the holes in the 4$^{th}$ element to produce approximately 15 %, 20 %, and 25 % reduction of the stiffness in the 4$^{th}$ element, respectively. These cases are referred to as Damage Scenarios III, IV and V, respectively.

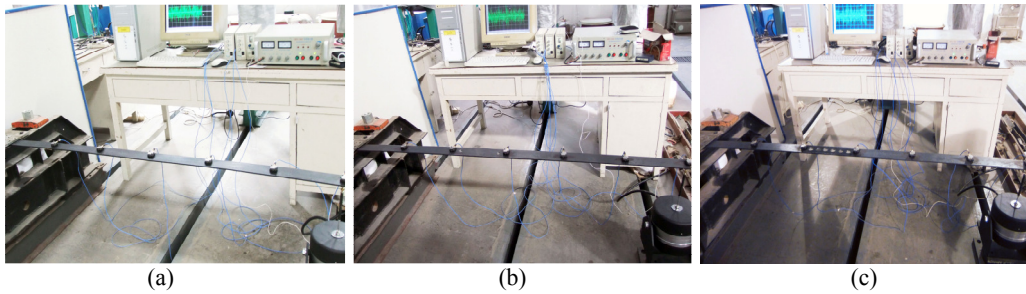

(a) (b) (c)

**Fig. 1.** Experimental setup and test specimens with constant damage: (a) Cantilever beam without damage, (b) Cantilever beam with small damage, (c) Cantilever beam with large damage

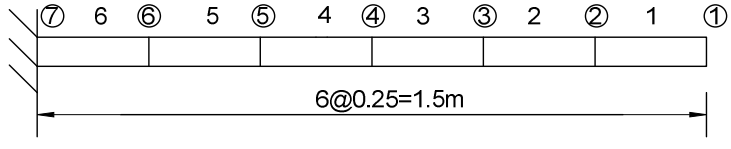


**Fig. 2.** Finite element model of the analyzed cantilever beam

### 3. 2 Reduced-order FE models

**12-DOF original FE model:** As shown in Fig. 2, the cantilever beam is divided into 6 elements with 6 evenly spaced nodal points. This results in a 12-DOF FE model, including 6 vertical displacements and 6 rotations at nodal points. Hence, the displacement vector $\underline{\mathbf{x}}(t) = [x_1, x_2, \ldots, x_6, x_7, \ldots, x_{12}]^{\mathrm{T}}$ consists of 12 elements, where the first 6 elements, $(x_1, x_2, \ldots, x_6)$, represent the vertical displacements and the last 6 elements, $(x_7, x_8, \ldots, x_{12})$, denote the rotations of the nodal points. The dimensions of the mass matrix $\underline{\mathbf{M}}$, damping matrix $\underline{\mathbf{C}}$, and stiffness matrix $\underline{\mathbf{K}}$ are (12×12). The Rayleigh damping is assumed so that $\underline{\mathbf{C}} = \alpha\underline{\mathbf{M}} + \beta\underline{\mathbf{K}}$, where $\alpha$ and $\beta$ are the proportional damping coefficients. The unknown parametric vector $\boldsymbol{\theta} = [k_1, k_2, k_3, k_4, k_5, k_6, \alpha, \beta]^{\mathrm{T}}$ of the structure consists of the stiffness of all finite elements and the proportional damping coefficients $\alpha$ and $\beta$. Here, the stiffness $k_i$ of the $i^{\mathrm{th}}$ finite element is defined as $k_i = E_i I_i / L_i$, where $E_i$, $I_i$, and $L_i$ are the Young's modulus, moment of inertia and length of the $i^{\mathrm{th}}$ element, respectively. To avoid the need for measuring the rotational accelerations at the nodal points, reduced-order systems, including a 6-DOF system and a 3-DOF system, will be established in the following for the purpose of damage detection.

**6-DOF reduced-order FE model:** In this model, we consider 6 vertical displacements as the primary DOFs, and 6 rotations as the secondary DOFs. Based on the static condensation method [20, 21], the 12-DOF FE model is condensed into a 6-DOF system with $\mathbf{x} = [x_1, x_2, x_3, x_4, x_5, x_6]^{\mathrm{T}}$, i. e., the rotational DOFs have been condensed. This reduced-order system along with the ASNLSE technique will be used to identify the damage in the cantilever beam.

**3-DOF reduced-order FE model:** Another reduced-order system to be considered is a 3-DOF system. In this model, we consider 3 vertical displacements as the primary DOFs, i.e. $x_1$, $x_4$, and $x_6$, and other 9 response quantities as the secondary DOFs. Based on the static condensation method [21] the 12-DOF FE model is condensed into a 3-DOF system with $\mathbf{x} = [x_1, x_4, x_6]^{\mathrm{T}}$. This reduced-order system will also be used for the damage detection.

### 3. 3 Experimental results and damage detection

As described above, five damage scenarios for the cantilever beam had been tested, representing approximately 5 %, 10 %, 15 %, 20 %, and 25 % stiffness reductions in the 4th element, respectively. The stiffness of each finite element for these five damage scenarios estimated based on the dimension of the specimen and the static analysis are shown in Table 1 to serve as reference values. During the experimental tests, vertical excitation in the form of a sinusoidal and white noise excitations, respectively, are applied to the first nodal point (Fig. 1). Six vertical accelerations at all nodal points were measured. The sampling frequency of all measurements is 500 Hz.

**Table 1.** Reference stiffness values for all finite elements

| Damage scenario | Stiffness | | | | | |
|---|---|---|---|---|---|---|
| | $k_1$ | $k_2$ | $k_3$ | $k_4$ | $k_5$ | $k_6$ |
| UD (undamaged) | 7.98 | 7.98 | 7.98 | 7.98 | 7.98 | 7.98 |
| I | 7.98 | 7.98 | 7.98 | 7.58 | 7.98 | 7.98 |
| II | 7.98 | 7.98 | 7.98 | 7.18 | 7.98 | 7.98 |
| III | 7.98 | 7.98 | 7.98 | 6.78 | 7.98 | 7.98 |
| IV | 7.98 | 7.98 | 7.98 | 6.38 | 7.98 | 7.98 |
| V | 7.98 | 7.98 | 7.98 | 5.99 | 7.98 | 7.98 |

For the identification of damages in the cantilever beam based on the sequential non-linear least-square estimation (ASNLSE), it is not necessary to use all the sensor measurements, i. e., $\ddot{x}_i$ ($i = 1, 2, \ldots, 6$) and $f$. Further, either the 6-DOF reduced-order system or the 3-DOF reduced order system can be used for the damage identification. Hence, the damage identification will be carried out using fewer measurements along with either the 3-DOF or the 6-DOF reduced-order system as shown in Table 2. Here the number of measurements used for damage identification is designated in the last column, whereas the damage scenario is shown in the second column. Consequently, we shall denote the damage identification cases (column 1 of Table 2) using both the roman letter (for damage scenarios) and the numeral letter (for the number of measurements used for the damage identification). For instance, the damage identification case I-7 (column 1 of Table 2) indicates the damage prediction for the damage scenario I (a stiffness reduction of about 5 % in the 4th finite element) using 7 measurements, i. e., $\ddot{x}_i$ ($i = 1, 2, \ldots, 6$) and $f$ (see Table 2(a)) based on 6-DOF reduced-order system. Likewise, damage identification case III-4UI indicates damage prediction for the damage scenario III (a stiffness reduction of about 15 % in the 4th finite element) using 4 measurements, i.e., $\ddot{x}_1$, $\ddot{x}_3$, $\ddot{x}_5$ and $\ddot{x}_6$, without the use of the measured excitation $f$ (input), see Table 2(a). Damage predictions for different damage scenarios using different number of measurements based on the 3-DOF reduced-order system are also shown in Table 2(b).

Recursive solutions given in Eqs. (6)-(15) will be used to identify the stiffness of each finite element of the cantilever beam. To start the recursive solutions, reasonable initial values for unknown quantities should be assumed, e. g., the stiffness and damping coefficients should be positive values. Here, the initial values for the state variables are taken to be zero. The initial values for $k_i$ ($i = 1, 2, \ldots, 6$), $\alpha$, $\beta$, are: $k_i = 3.5$ kN/m ($i = 1, 2, \ldots, 6$), $\alpha = 0$ s$^{-1}$, $\beta = 0$ s. The initial value of the variance matrix of the measurement noise vector is assumed to be $\mathbf{R} = \mathbf{I}_6$.

Based on different reduced-order systems with different numbers of sensor measurements, the stiffness of all finite elements of the cantilever beam were identified using the recursive solutions in Eqs. (7)-(8). The identified results are presented in Table 3 for the white noise

excitations. The results for the sinusoidal excitations are very similar to that presented in Table 3, and hence they are not shown. Also presented in Table 3 for comparison are the reference values, which are obtained based on the dimension of the test specimen and the static analysis given in Table 1. It is observed from Table 3 that: (i) the predicted stiffness of all elements is quite close to the reference values, and (ii) the location and severity of the structural damage can be identified accurately.

**Table 2.** Damage identification cases for constant damages

| (a) 6-DOF | | |
|---|---|---|
| Case No. | Damage scenario | Number of measurements used |
| UD-7 | Undamaged | 7 ($\ddot{x}_1$, $\ddot{x}_2$, $\ddot{x}_3$, $\ddot{x}_4$, $\ddot{x}_5$, $\ddot{x}_6$, $f$) |
| I-7 | I | 7 ($\ddot{x}_1$, $\ddot{x}_2$, $\ddot{x}_3$, $\ddot{x}_4$, $\ddot{x}_5$, $\ddot{x}_6$, $f$) |
| II-7 | II | 7 ($\ddot{x}_1$, $\ddot{x}_2$, $\ddot{x}_3$, $\ddot{x}_4$, $\ddot{x}_5$, $\ddot{x}_6$, $f$) |
| III-7 | III | 7 ($\ddot{x}_1$, $\ddot{x}_2$, $\ddot{x}_3$, $\ddot{x}_4$, $\ddot{x}_5$, $\ddot{x}_6$, $f$) |
| IV-7 | IV | 7 ($\ddot{x}_1$, $\ddot{x}_2$, $\ddot{x}_3$, $\ddot{x}_4$, $\ddot{x}_5$, $\ddot{x}_6$, $f$) |
| V-7 | V | 7 ($\ddot{x}_1$, $\ddot{x}_2$, $\ddot{x}_3$, $\ddot{x}_4$, $\ddot{x}_5$, $\ddot{x}_6$, $f$) |
| III-6UI | III | 6 ($\ddot{x}_1$, $\ddot{x}_2$, $\ddot{x}_3$, $\ddot{x}_4$, $\ddot{x}_5$, $\ddot{x}_6$) |
| IV-6UI | IV | 6 ($\ddot{x}_1$, $\ddot{x}_2$, $\ddot{x}_3$, $\ddot{x}_4$, $\ddot{x}_5$, $\ddot{x}_6$) |
| IV-5UI | IV | 5 ($\ddot{x}_1$, $\ddot{x}_3$, $\ddot{x}_4$, $\ddot{x}_5$, $\ddot{x}_6$) |
| III-4UI | III | 4 ($\ddot{x}_1$, $\ddot{x}_3$, $\ddot{x}_5$, $\ddot{x}_6$) |
| IV-3UI | IV | 3 ($\ddot{x}_1$, $\ddot{x}_3$, $\ddot{x}_5$) |
| (b) 3-DOF | | |
| Case No. | Damage scenario | Number of measurements used |
| UD-4 | Undamaged | 4 ($\ddot{x}_1$, $\ddot{x}_4$, $\ddot{x}_6$, $f$) |
| I-4 | I | 4 ($\ddot{x}_1$, $\ddot{x}_4$, $\ddot{x}_6$, $f$) |
| II-4 | II | 4 ($\ddot{x}_1$, $\ddot{x}_4$, $\ddot{x}_6$, $f$) |
| III-4 | III | 4 ($\ddot{x}_1$, $\ddot{x}_4$, $\ddot{x}_6$, $f$) |
| IV-4 | IV | 4 ($\ddot{x}_1$, $\ddot{x}_4$, $\ddot{x}_6$, $f$) |
| V-4 | V | 4 ($\ddot{x}_1$, $\ddot{x}_4$, $\ddot{x}_6$, $f$) |
| III-3UI | III | 3 ($\ddot{x}_1$, $\ddot{x}_4$, $\ddot{x}_6$) |

To further demonstrate the accuracy of the damage identification technique presented, consider the damage identification case IV-3UI based on the 6-DOF reduced-order system (Table 2(a)). In this case, white noise excitation $f$ (input) and the vertical acceleration responses $\ddot{x}_2$, $\ddot{x}_4$ and $\ddot{x}_6$ of the 2nd, 4th and 6th nodal points are not used in the damage prediction. Here, the ASNLSE technique is capable of identifying the unknown excitations (input). The identified unknown excitation $f$ is presented in Fig. 3 as a solid curve, whereas the experimentally measured excitation is shown in the same figure as a dashed curve for comparison. Further, based on the 3-DOF reduced-order system, we consider the damage identification case III-3UI, Table 2(b). In this case, only the measured acceleration responses, $\ddot{x}_2$, $\ddot{x}_4$ and $\ddot{x}_6$, were used for the damage prediction without the use of the external excitation. The identified unknown white noise excitation is presented in Fig. 4 as a solid curve, whereas the measured excitation is shown in the same figure as a dashed curve for comparison. It is observed from Figs. 3 and 4 that the correlations between the predicted unknown excitations and the measured excitations are very plausible.

**Table 3.** Identified stiffness results (kN/m)

| Case No. | | $k_1$ | $k_2$ | $k_3$ | $k_4$ | $k_5$ | $k_6$ |
|---|---|---|---|---|---|---|---|
| (a) 6-DOF | | | | | | | |
| UD-7 | reference values | 7.98 | 7.98 | 7.98 | 7.98 | 7.98 | 7.98 |
| | identified values | 8.05 | 7.85 | 7.86 | 7.86 | 7.86 | 7.82 |
| | difference (%) | +0.88 | -1.63 | -1.50 | -1.50 | -1.50 | -2.01 |
| I-7 | reference values | 7.98 | 7.98 | 7.98 | 7.58 | 7.98 | 7.98 |
| | identified values | 7.86 | 8.05 | 7.81 | 7.64 | 7.82 | 7.82 |
| | difference (%) | -1.50 | +0.88 | -2.13 | +0.79 | -2.01 | -2.01 |
| II-7 | reference values | 7.98 | 7.98 | 7.98 | 7.18 | 7.98 | 7.98 |
| | identified values | 7.88 | 7.86 | 7.84 | 7.09 | 7.86 | 7.81 |
| | difference (%) | -1.25 | -1.50 | -1.75 | -1.25 | -1.50 | -2.13 |
| III-7 | reference values | 7.98 | 7.98 | 7.98 | 6.78 | 7.98 | 7.98 |
| | identified values | 7.81 | 7.84 | 7.87 | 6.85 | 7.89 | 7.82 |
| | difference (%) | -2.13 | -1.75 | -1.38 | +1.03 | -1.13 | -2.01 |
| IV-7 | reference values | 7.98 | 7.98 | 7.98 | 6.38 | 7.98 | 7.98 |
| | identified values | 7.83 | 7.82 | 7.86 | 6.35 | 7.85 | 7.87 |
| | difference (%) | -1.88 | -2.01 | -1.50 | -0.47 | -1.63 | -1.38 |
| V-7 | reference values | 7.98 | 7.98 | 7.98 | 5.99 | 7.98 | 7.98 |
| | identified values | 7.86 | 7.85 | 7.83 | 5.92 | 7.82 | 7.84 |
| | difference (%) | -1.50 | -1.63 | -1.88 | -1.17 | -2.01 | -1.75 |
| III-6UI | reference values | 7.98 | 7.98 | 7.98 | 6.78 | 7.98 | 7.98 |
| | identified values | 7.82 | 7.86 | 7.91 | 6.75 | 7.89 | 7.86 |
| | difference (%) | -2.01 | -1.50 | -0.88 | -0.44 | -1.13 | -1.50 |
| IV-6UI | reference values | 7.98 | 7.98 | 7.98 | 6.38 | 7.98 | 7.98 |
| | identified values | 7.87 | 7.85 | 7.91 | 6.35 | 7.87 | 7.86 |
| | difference (%) | 1.38 | 1.63 | 0.88 | 0.47 | 1.38 | 1.50 |
| IV-5UI | reference values | 7.98 | 7.98 | 7.98 | 6.38 | 7.98 | 7.98 |
| | identified values | 7.85 | 7.83 | 7.89 | 6.32 | 7.93 | 7.88 |
| | difference (%) | 1.63 | 1.88 | 1.13 | 0.94 | 0.63 | 1.25 |
| III-4UI | reference values | 7.98 | 7.98 | 7.98 | 6.78 | 7.98 | 7.98 |
| | identified values | 7.86 | 7.82 | 7.83 | 6.76 | 7.91 | 7.89 |
| | difference (%) | -1.50 | -2.01 | -1.88 | -0.29 | -0.88 | -1.13 |
| IV-3UI | reference values | 7.98 | 7.98 | 7.98 | 6.38 | 7.98 | 7.98 |
| | identified values | 7.93 | 7.91 | 7.89 | 6.32 | 7.86 | 7.81 |
| | difference (%) | 0.63 | 0.88 | 1.13 | 0.94 | 1.50 | 2.13 |
| (b) 3-DOF | | | | | | | |
| UD-4 | reference values | 7.98 | 7.98 | 7.98 | 7.98 | 7.98 | 7.98 |
| | identified values | 7.82 | 7.89 | 7.91 | 7.85 | 7.86 | 7.87 |
| | difference (%) | -2.01 | -1.13 | -0.88 | -1.63 | 1.50 | -1.38 |
| I-4 | reference values | 7.98 | 7.98 | 7.98 | 7.58 | 7.98 | 7.98 |
| | identified values | 7.86 | 7.85 | 7.87 | 7.49 | 7.91 | 7.89 |
| | difference (%) | -1.50 | -1.63 | -1.38 | -1.19 | -0.88 | -1.13 |
| II-4 | reference values | 7.98 | 7.98 | 7.98 | 7.18 | 7.98 | 7.98 |
| | identified values | 7.87 | 7.86 | 7.93 | 7.09 | 7.88 | 7.86 |
| | difference (%) | -1.38 | -1.50 | -0.63 | -1.25 | -1.25 | -1.50 |
| III-4 | reference values | 7.98 | 7.98 | 7.98 | 6.78 | 7.98 | 7.98 |
| | identified values | 7.85 | 7.86 | 7.83 | 6.71 | 7.87 | 7.86 |
| | difference (%) | -1.63 | -1.50 | -1.88 | -1.03 | -1.38 | -1.50 |
| IV-4 | reference values | 7.98 | 7.98 | 7.98 | 6.38 | 7.98 | 7.98 |
| | identified values | 7.87 | 7.95 | 7.89 | 6.31 | 7.85 | 7.86 |
| | difference (%) | -1.38 | -0.38 | -1.13 | -1.10 | -1.63 | -1.50 |
| V-4 | reference values | 7.98 | 7.98 | 7.98 | 5.99 | 7.98 | 7.98 |
| | identified values | 7.86 | 7.89 | 7.88 | 5.93 | 7.91 | 7.89 |
| | difference (%) | -1.50 | -1.13 | -1.25 | -1.00 | -0.88 | -1.13 |
| III-3UI | reference values | 7.98 | 7.98 | 7.98 | 6.78 | 7.98 | 7.98 |
| | identified values | 7.85 | 7.88 | 7.85 | 6.72 | 7.87 | 7.87 |
| | difference (%) | -1.63 | -1.25 | -1.25 | -0.88 | -1.38 | -1.38 |


© VIBROENGINEERING. JOURNAL OF VIBROENGINEERING. SEPTEMBER 2012. VOLUME 14, ISSUE 3. ISSN 1392-8716

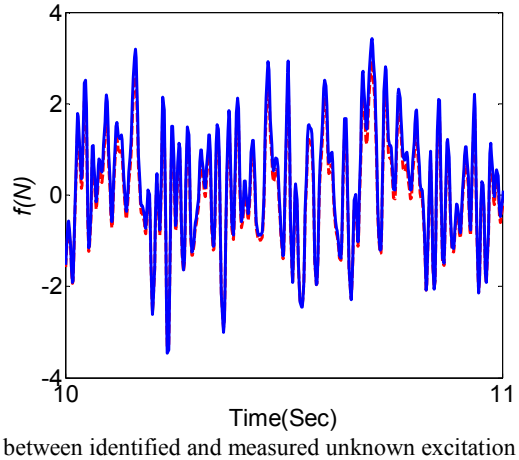


**Fig. 3.** Comparison between identified and measured unknown excitation forces for case IV-3UI (6-DOF reduced-order system)

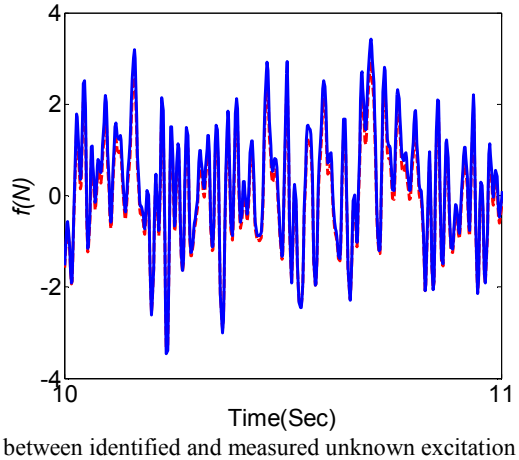


**Fig. 4.** Comparison between identified and measured unknown excitation forces for case III-3UI

## 4. Experimental studies for online damage tracking

To demonstrate the online parametric tracking capability of the proposed approach, experiments were conducted using another cantilever beam. The dimension of this cantilever beam (length and cross-sectional area) was identical to that shown in Fig. 1, and the beam was divided into 6 evenly spaced nodal points. Each nodal point was installed with an acceleration sensor to measure the vertical acceleration. An actuator was used to apply the external excitation force at the end node, and a force sensor (PCB 208C03) was used to measure the applied force. For this cantilever beam, a stiffness element device (SED) was installed in the 3rd finite element to increase the stiffness of that element by an amount $k_e$ as shown in Figs. 5 and 6. At a particular time instant $t_r$ during the experimental test, the stiffness of the SED was abruptly reduced by an amount $\Delta k_e$ as will be explained in the following. The capability of the proposed damage identification approach, i.e. the use of ASNLSE and the reduced order system, to track the variation of the element stiffness at the time instant $t_r$ will be demonstrated experimentally.

Consider a device consisting of a hydraulic cylinder-piston (HCP) unit with one valve on each side of the piston as shown in Fig. 7. With both valves being closed, the cylinder is filled with pressurized gas. Hence, the HCP serves as a stiffness element in which the stiffness is

provided by the bulk modulus of the pressurized gas in the cylinder. When both valves are open, the piston is free to move and the stiffness of the HCP becomes zero. For simulating the stiffness reduction in a selected finite element, the HCP is connected to a bracing system and installed in the selected finite element as shown in Fig. 6. The entire system, consisting of a HCP and a bracing system is referred to as the stiffness element device (SED). To simulate the reduction of stiffness in the $i^{th}$ element, a SED with both valves closed is installed in the $i^{th}$ element, so that the stiffness of the $i^{th}$ element is increased. During the experimental test, two valves in the HCP are open simultaneously at the time instant $t_r$, so that the stiffness of the $i^{th}$ element will be reduced at $t = t_r$ by an amount $\Delta k_e$. In this test series, the SED was installed in the 3rd finite element as shown in Figs. 5 and 6.

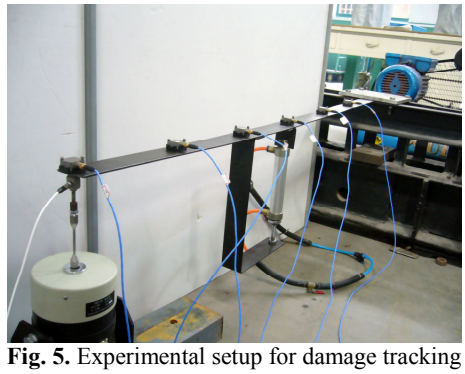

**Fig. 5.** Experimental setup for damage tracking

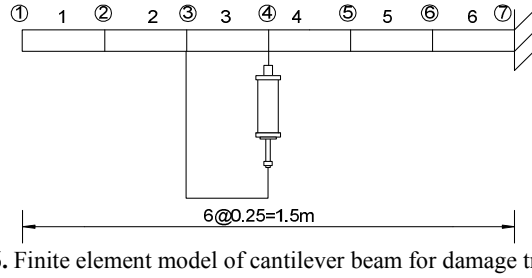


**Fig. 6.** Finite element model of cantilever beam for damage tracking

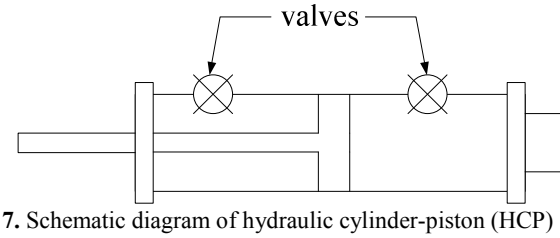


**Fig. 7.** Schematic diagram of hydraulic cylinder-piston (HCP) system

To determine the reference stiffness values of all finite elements of the beam equipped with the SED in the 3rd finite element, cantilever beams with valves closed (without damage) and with valves open (damaged case) were tested separately. Firstly, both valves of the HCP were closed and the cylinder was filled with air at an air pressure of 0.8 MPa. SED system was installed in the 3rd element and a vertical excitation in the form of a white noise excitation was applied at the 1st nodal point of the beam. Six vertical accelerations at all nodal points were measured with a sampling frequency of 500 Hz. Based on the ASNLSE and the 6-DOF reduced-

order system, the stiffness of all finite elements was predicted using all 6 acceleration measurements and the measured excitation force. The results are shown in Table 4 ($t \leq 10$ seconds) and Fig. 8(a), referred to as the reference values of all finite elements when both valves in HCP were closed, simulating the beam without damage. Note that the same initial values as the previous predictions had been used except that $k_3 = 10$ kN/m. As observed from Table 4, the stiffness of the 3rd finite element increases from 7.71 kN/m to 22.22 kN/m, an increase of $k_e = 14.51$ kN/m due to the installation of the SED.

**Table 4.** Reference stiffness values (kN/m) for damage tracking

| Element number | | $k_1$ | $k_2$ | $k_3$ | $k_4$ | $k_5$ | $k_6$ |
|---|---|---|---|---|---|---|---|
| Valves closed | $t \leq 10$ s | 7.71 | 7.71 | 22.22 | 7.71 | 7.71 | 7.71 |
| Values open | $t > 10$ s | 7.72 | 7.71 | 19.11 | 7.71 | 7.71 | 7.71 |

Secondly, two valves of the HCP were opened and the air pressure in the cylinder was zero, simulating the beam with damage. Repeating the same experiment as above, the stiffness of all finite elements were predicted, and the results are shown in Table 4 ($t \leq 10$ seconds) and Fig. 8(b). It is observed from Table 4 that the stiffness of the 3rd finite element is 19.11 kN/m. In comparison with the undamaged beam, the stiffness of the 3rd element is reduced by $\Delta k_e = 22.22 - 19.11 = 3.11$ kN/m. It is further observed from Fig. 8 that the recursive solutions for the stiffness of the damaged and undamaged beams converge rapidly and nicely.

Now, the two valves in the SED were closed and the cylinder was filled with air at an air pressure of 0.8 MPa. SED was installed in the 3rd finite element of the cantilever beam and a vertical white noise excitation force was applied at the first nodal point (Fig. 5). At the time instant $t_r = 10$ seconds during the test, two valves in the SED were open simultaneously, so that the air pressure became zero, and the test was continued until 30 seconds. Acceleration responses of all nodal points and the excitation force were recorded. The capability of the proposed damage detection method to track the variation of the stiffness of all elements at $t_r = 10$ seconds will be demonstrated.

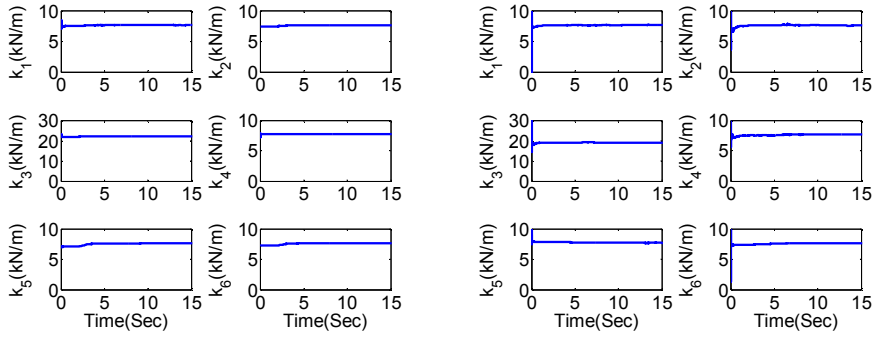


**Fig. 8.** Reference stiffness values: (a) undamaged beam, and (b) damaged beam

As discussed in the previous section, the ASNLSE approach does not need all the acceleration response records nor does it require the measured excitation force. Hence, the damage tracking will be carried out using fewer measurements as well as 6-DOF or 3-DOF reduced-order systems as shown in Table 5. Here the number of sensor measurements used for the damage tracking is designated by the numeral letter in the last column and the damage tracking case is shown in the first column. For instance, the case 6DOF-3UI indicates the damage tracking based on the 6-DOF reduced-order system using only 3 measured acceleration

responses $(\ddot{x}_1, \ddot{x}_3, \ddot{x}_5)$ without the excitation record. Further, the case 3DOF-3UI denotes the damage tracking based on the 3-DOF reduced-order system using only 3 measured acceleration responses $(\ddot{x}_1, \ddot{x}_4, \ddot{x}_6)$ without the excitation record.

**Table 5.** Identification cases for damage tracking

| Case No. | Number of measurements used |
|---|---|
| 6DOF-7 | 7 $(\ddot{x}_1, \ddot{x}_2, \ddot{x}_3, \ddot{x}_4, \ddot{x}_5, \ddot{x}_6, f)$ |
| 6DOF-6UI | 6 $(\ddot{x}_1, \ddot{x}_2, \ddot{x}_3, \ddot{x}_4, \ddot{x}_5, \ddot{x}_6)$ |
| 6DOF-5UI | 5 $(\ddot{x}_1, \ddot{x}_3, \ddot{x}_4, \ddot{x}_5, \ddot{x}_6)$ |
| 6DOF-4UI | 4 $(\ddot{x}_1, \ddot{x}_3, \ddot{x}_5, \ddot{x}_6)$ |
| 6DOF-3UI | 3 $(\ddot{x}_1, \ddot{x}_3, \ddot{x}_5)$ |
| 3DOF-4 | 4 $(\ddot{x}_1, \ddot{x}_4, \ddot{x}_6, f)$ |
| 3DOF-3UI | 3 $(\ddot{x}_1, \ddot{x}_4, \ddot{x}_6)$ |

Based on the recursive solutions in Eqs. (7) and (8), the time-varying stiffness of all finite elements of the beam had been predicted for all cases shown in Table 5. The damage tracking results for case 6DOF-7 is presented in Fig. 9 as solid curves, whereas the results for case 6DOF-4UI are displayed in Fig. 10 as solid curves. Also dashed curves in Figs. 9 and 10 are the reference values in Table 4 for comparison. Since no external excitation force was used for the damage tracking for case 6DOF-4UI, the predicted external excitation force is presented in Fig. 11 as a solid curve, whereas the measured record is shown in the same figure as a dashed curve for comparison. Further, the damage tracking results for case 3DOF-3UI is presented in Fig. 12 as solid curves, whereas the dashed curves are the reference values in Table 4 for comparison. The predicted external excitation force is presented in Fig. 13 as a solid curve, whereas the measured record is shown in the same figure as a dashed curve for comparison.

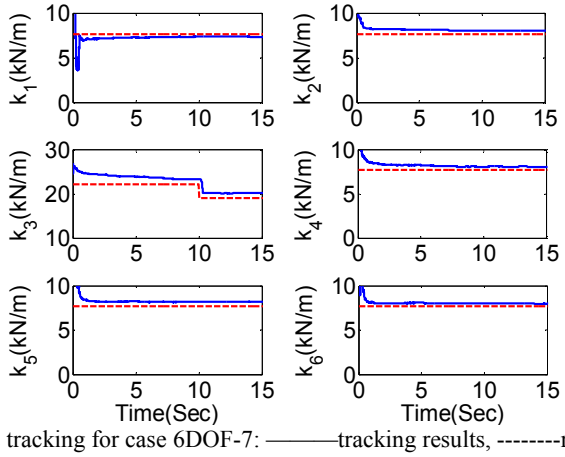


**Fig. 9.** Stiffness tracking for case 6DOF-7: ———tracking results, --------reference values

It is observed from Figs. 9-13 that: (i) the damage tracking for the stiffness of all elements is quite accurate, although only as few as 3 sensor measurements were used in the prediction, and (ii) the prediction for the unknown external excitation correlates very well with the measured one. Damage tracking for all cases in Table 5 has been conducted and the results are very similar to those presented in Figs. 8-13 (therefore, they are not shown). Finally, experiments using the sinusoidal excitation force had been conducted and damage tracking predictions had also been made. Since the results are also very similar to Figs. 9-13, they are not presented here.

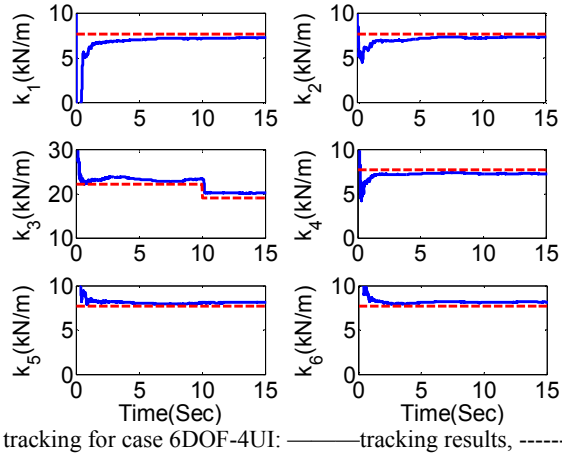


**Fig. 10.** Stiffness tracking for case 6DOF-4UI: ———tracking results, --------reference values

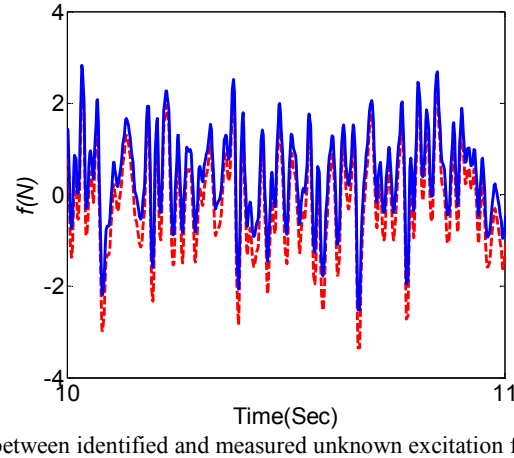


**Fig. 11.** Comparison between identified and measured unknown excitation forces for case 6DOF-4UI: ———tracking results, --------reference values

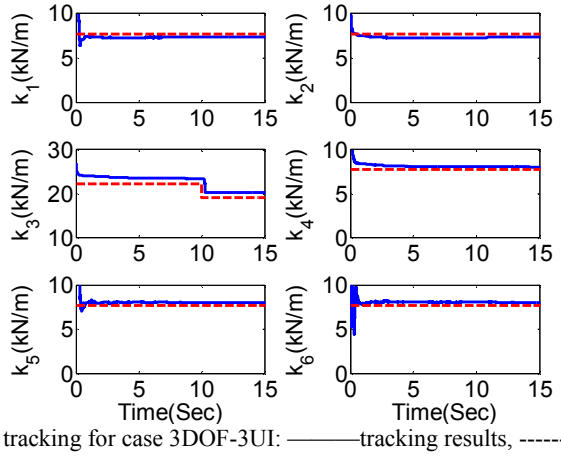


**Fig. 12.** Stiffness tracking for case 3DOF-3UI: ———tracking results, --------reference values

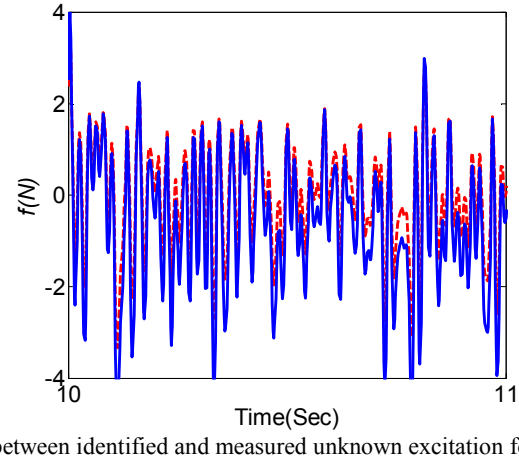


**Fig. 13.** Comparison between identified and measured unknown excitation forces for case 3DOF-3UI

## 5. Conclusions

A reduced-order FE formulation along with the adaptive sequential nonlinear least square estimation (ASNLSE) technique has been proposed in this paper in order to identify local damage of a structure at the element level using only a limited number of sensors. Two series of damage detection experiments have been conducted using scaled cantilever beams in order to verify the applicability and effectiveness of the proposed approach. One series of experimental tests were conducted for the detection of constant damages, whereas another series of experimental tests were conducted to verify the damage tracking capability of the proposed approach. Experimental results demonstrate that the proposed reduced-order FE model along with ASNLSE technique is effective and accurate in: (i) detecting constant structural damages, including the damage location and severity, and (ii) tracking time-varying structural parameters.

## Acknowledgments

This research is partially supported by the National Natural Science Foundation of China under Grant No. 10572058, the Science Foundation of Aeronautics of China under Grant No. 2008ZA52012, and US National Science Foundation Grant No. CMMI-0853395.

## References

**[1] Doebling S. W., Farrar C. R., Prime M. B.** A summary review of vibration-based damage identification method. Shock & Vibration Digest, 30(2), 1998, p. 91-105.

**[2] Alvin K. F., Robertson A. N., Reich G. W., Park K. C.** Structural system identification: from reality to models. Computers & Structures, 81(12), 2003, p. 1149-1176.

**[3] Bernal D., Beck J.** Special section: Phase I of the IASC-ASCE structural health monitoring benchmark. Journal of Engineering Mechanics, 130(1), 2004, p. 1-127.

**[4] Loh C. H., Lin C. Y., Huang C. C.** Time domain identification of frames under earthquake loadings. Journal of Engineering Mechanics, 126(7), 2000, p. 693-703.

**[5] Lin J. W., Betti R., Smyth A. W., Longman R. W.** On-line identification of nonlinear hysteretic structural systems using a variable trace approach. Earthquake Engineering and Structural Dynamics, 30(9), 2001, p. 1279-1303.

**[6] Smyth A. W., Masri S. F., Kosmatopoulos E. B., Chassiakos A. G., Caughey T. K.** Development of adaptive modeling techniques for non-linear hysteretic systems. International Journal of Non-Linear Mechanics, 37(8), 2002, p. 1435-1451.

**[7] Yang J. N., Lin S.** Identification of parametric variations of structures based on least square estimation and adaptive tracking technique. Journal of Engineering Mechanics, 131(3), 2005, p. 290-298.

**[8] Yang J. N., Pan S., Lin S.** Least square estimation with unknown excitations for damage identification of structures. Journal of Engineering Mechanics, 133(1), 2007, p. 12-21.

**[9] Sato T., Honda R., Sakanoue T.** Application of adaptive Kalman filter to identify a five story frame structure using NCREE experimental data. Proceedings of Structural Safety and Reliability, CA, U.S.A., 2001.

**[10] Yang J. N., Lin S., Huang H., Zhou L.** An adaptive extended Kalman filter for structural damage identification. Journal of Structural Control and Health Monitoring, 13(4), 2006, p. 849-867.

**[11] Yang J. N., Pan S., Huang H.** An adaptive extended Kalman filter for structural damage identification II: unknown inputs. Journal of Structural Control and Health Monitoring, 14(3), 2007, p. 497-521.

**[12] Zhou L., Wu S., Yang J. N.** Experimental study of an adaptive extended Kalman filter for structural damage identification. ASCE Journal of Infrastructure Systems, 14(1), 2008, p. 42-51.

**[13] Yoshida I., Sato T.** Health monitoring algorithm by the Monte Carlo filter based on non-Gaussian noise. Journal of National Disaster Science, 24(2), 2002, p. 101-107.

**[14] Tanaka Y., Sato T.** Efficient system identification algorithm using Monte Carlo filter and its applications. Proceeding of SPIE, U.S.A., 2004.

**[15] Goodwin C. G., Sin K. S.** Adaptive Filtering Prediction and Control. Information and System Science Series, 1984.

**[16] Yun C. B., Lee H. J., Lee C. G.** Sequential prediction error method for structural identification. Journal of Engineering Mechanics, 123(2), 1997, p. 115-123.

**[17] Ching J., Beck J. L., Porter K. A., Shaikhutdinov R.** Bayesian state estimation method for nonlinear systems and its application to recorded seismic response. Journal of Engineering Mechanics, 132(4), 2006, p. 396-410.

**[18] Yang J. N., Huang H.** Sequential non-linear least-square estimation for damage identification of structures. International Journal of Non-Linear Mechanics, 41(1), 2006, p. 124-140.

**[19] Yang J. N., Huang H.** Sequential non-linear least-square estimation for damage identification of structures with unknown inputs and unknown outputs. International Journal of Non-Linear Mechanics, 42(5), 2007, p. 789-801.

**[20] Guyan R. J.** Reduction of stiffness and mass matrices. AIAA Journal, 3(2), 1965, p. 380-380.

**[21] Chopra A. K.** Dynamics of Structures, Theory and Applications to Earthquake Engineering. Prentice-Hall Inc., New Jersey, USA, 2001.